# BPA-Containing Polydopamine Nanoparticles for Boron Neutron Capture Therapy in a U87 Glioma Orthotopic Model

*Liqun Dai, Jie Liu, Xiaosheng Zhao, Yuhao Li, Siming Zhou, Liping Yuan, Diyun Shu, Lili Pan, Yuan-hao Liu, and Zhiyong Qian\**

Boron neutron capture therapy (BNCT) is a promising therapy for refractory cancer based on the cytotoxic reaction of $^{10}B$ (n, $\alpha$) $^7Li$. Although two BNCT agents are clinically available, they are quickly metabolized and show modest enrichment in tumor sites, partially limiting BNCT widespread application. Consequently, novel agents that perform active targeting and show good biocompatibility have to be developed. Herein, boronophenylalanine-containing polydopamine (B-PDA) nanoparticles are easily fabricated by encapsulating boronophenylalanine (BPA) in polydopamine via nitrogen-boronate coordination. In this study, B-PDA achieves increased tumor accumulation and prolonged retention effects in the tumor site and superior antitumor activity post neutron irradiation in the orthotopic xenograft glioma model. In brief, this study offers a novel strategy for BPA delivery and may broaden the perspective on nanomedicine design for BNCT.

## 1. Introduction

As an advanced binary system for treating unresectable cancer, boron neutron capture therapy (BNCT) is a modality of cell-selective radiotherapy that utilizes lithium nuclei and alpha particles, which are produced by the boron neutron capture reaction.[1] In addition, these particles typically have a very short range, travelling just tens of micrometres; they provide a mode to selectively destroy tumor cells while sparing normal cells and exhibit the potential for treating various types of cancers.[2,3]

In summary, BNCT is a combination of boron-containing drugs and neutron beams.[2,4,5] BNCT was initially performed mainly at reactor sites,[6] for example, ≈240 patients underwent BNCT at the BNCT centre in Helsinki University Hospital, Finland, from 1999 to 2012.[2,7] Today, due to efforts from different scientific research groups, accelerator-driven BNCT facilities have been constructed worldwide; among them, several accelerators for BNCT have been evaluated or are being evaluated in clinical trials in Japan,[8] Finland,[9] the United States of America,[10] Taiwan,[11] etc.

In addition, one of the essential requirements for BNCT drugs is their ability to accumulate selectively in cancer cells.[12] However, at present, only two agents are available for clinical BNCT applications;[13–15] of these, boronophenylalanine (BPA) is a phenylalanine derivative containing B-10 and can be taken up by cells via L-type amino acid transporters.[14] As an amino acid derivative, BPA shows high biosafety and has been considered the most reliable BNCT agent by far, but its fast metabolism and modest enrichment in tumor sites partly limit the widespread use of BPA for BNCT.[16] Thus, researching and developing active-selective medications are paramount endeavours.

More recently, to overcome the limitations of BNCT agents by increasing drug accumulation and prolonging drug retention in tumor sites, the nanomedicines used for BNCT have received significant attention.[14,17] For example, a BPA-decorated polymeric nanoparticle has been reported,[18,19] while the phenylalanine residues showed high affinity and selectively for sialic acid contained in sialylated antigen to achieve enrichment in the tumor region. In addition, boron-containing carbon dots were coated into exosomes to prepare BCD-Exo formulations for glioma tumor BNCT with significant therapeutic effects.[20] These studies unambiguously have demonstrated that the BPA nanocomponents still displayed superior performance in the treatment of tumor models. Although the initial results are encouraging, these agents are far from achieving clinical application, and more efficient and safer BNCT nanodrugs are worthy of future investigation.

Based on the evidence mentioned above, herein, we report the design and synthesis of novel BPA-containing polydopamine (B-PDA) nanoparticles for BNCT to treat U87 tumor-bearing

L. Dai, J. Liu, X. Zhao, S. Zhou, L. Yuan, Z. Qian
State Key Laboratory of Biotherapy and Cancer Center
West China Hospital
West China Medical School
Sichuan University
Collaborative Innovation Center of Biotherapy
Chengdu 610041, China
E-mail: zhiyongqian@scu.edu.cn
Y. Li, L. Pan
Laboratory of Clinical Nuclear Medicine
Department of Nuclear Medicine
West China Hospital, Sichuan University
Chengdu 610041, China
D. Shu, Y.-h. Liu
Nanjing University of Aeronautics and Astronautics
Nanjing, Jiangsu 210016, China
D. Shu, Y.-h. Liu
Neuboron Medtech Ltd.
Nanjing, Jiangsu 211112, China

The ORCID identification number(s) for the author(s) of this article can be found under https://doi.org/10.1002/adfm.202214145.
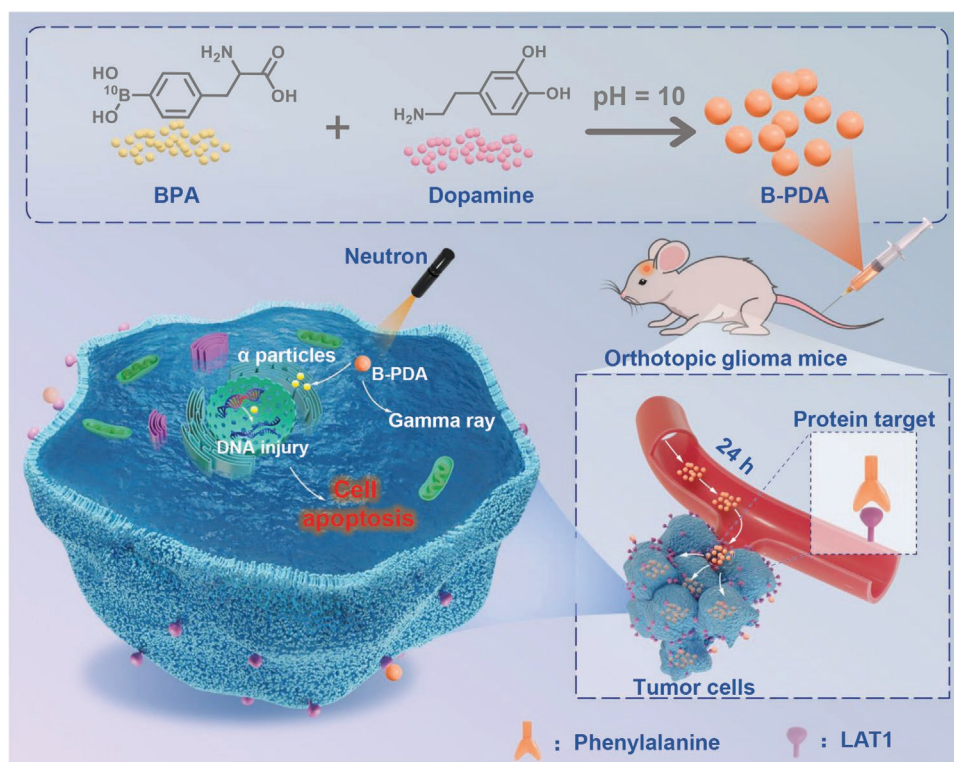
**Figure 1.** Schematic illustration of the B-PDA nanoparticle formula and the application of boron neutron capture therapy in a tumor mouse model.
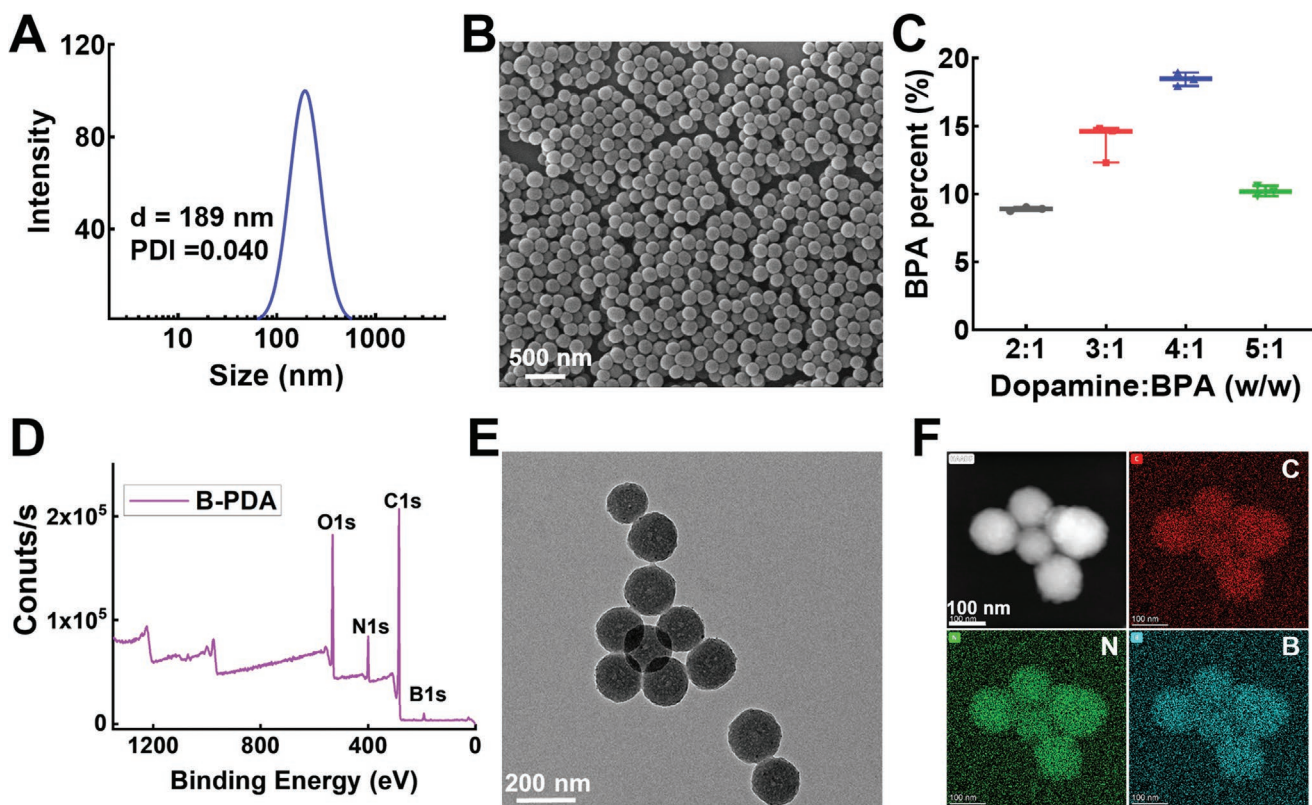
mice (**Figure 1**). To fabricate the nanocomposites, a reaction mixture of BPA and dopamine was stirred overnight under basic aqueous conditions at room temperature. The formed products also exhibited the phenylalanine residue of BPA, which can recognize the neutral amino acid transporter L-type amino acid transporter 1 (LAT1).[15,21] LAT1, as a high-affinity amino acid transporter, was overexpressed in the blood-brain barrier; thus, B-PDA can cross the blood-brain barrier and might be used for glioma BNCT. In this study, U87 cells were used as the experimental cells. U87 cell, as a human-derived malignant glioma cell line, is one of the most widely used glioma cell lines and is a good candidate for in vitro and in vivo models. The U87 glioma orthotopic model is an appropriate model for studying antitumor angiogenesis and the high recurrence rate of glioma with an entirely abnormal and leaky vasculature, which is suitable for nanomedicine research.[22,23] A previous study indicated that phenylalanine could recognize LAT1 in U87 cells to promote complex uptake.[24] Thus, due to the combined passive targeting and LAT1-mediated active targeting effects, more B-PDA accumulation in tumor cells is promising. Then, we detected the peak boron concentration (29.68 ± 2.23 ppm) in the tumor site at 24 h postinjection, which was accompanied by the maximum tumor-to-brain ratio (7.60 ± 1.91). Moreover, the B-PDA nanoparticles contain various active groups, and some modifications can be carried out, such as grafting the fluorescent probe Cy5. In vivo fluorescence imaging indicated that B-PDA nanoparticles could enter tumor cells, which suggested that B-PDA might be favored for BNCT. Finally, efficacy was evaluated with orthotopic glioma mice; as expected, the results indicated that B-PDA provided an ideal platform for BNCT to combat cancer. Overall, the B-PDA nanoparticles show potential as agents for BNCT in the U87 glioma orthotopic model.

## 2. Results and Discussion

### 2.1. Preparation and Characterization of B-PDA

In this work, a series of BPA-PDA nanoparticles were fabricated via a one-step process and purified by centrifugation. When the dopamine/BPA mass ratios were increased from 2:1 to 5:1, BPA-PDA nanoparticles with different BPA percentages were prepared, but when dopamine and BPA were in a 1:1 ratio, no particles were formed in the same procedure. DLS and SEM experimental results are included in Figure S2A,B (Supporting Information) and **Figure 2**A,B. The preliminary findings indicated that the method can be applied to prepare BPA-containing PDA nanoparticles, but the BPA percent in nanoparticles was unclear. To further study this, the subtype differences in nanoparticles were calculated by ICP-MS, as shown in Table S1 (Supporting Information) and Figure 2C. From ICP-MS, it was shown that the BPA percent of BPA-PDA was 8.90 ± 0.14%, 14.09 ± 0.61%, and 10.49 ± 0.83% when the mass ratio of dopamine and BPA was 2:1, 3:1, and 5:1, respectively. The largest percent (18.73 ± 0.40%) of BPA was achieved at a mass ratio of 4:1 (dopamine/BPA); therefore, we adopted this ratio for subsequent studies. The B-PDA particles formed in this way, perhaps due to the formation of boronate ester between the amino groups of dopamine and the boronic acid structure of BPA.[25,26] To further demonstrate the absence of boronate ester, we used FT-IR spectroscopy to estimate the

ADVANCED
SCIENCE NEWS
www.advancedsciencenews.com

ADVANCED
FUNCTIONAL
MATERIALS
www.afm-journal.de

**Figure 2.** Physiochemical property characterization of B-PDA nanoparticles. A) DLS analysis and B) SEM image of nanoparticles prepared by dopamine and BPA in a mass ratio of 4:1; C) Quantitative analysis of the BPA contents in BPA-PDA nanoparticles by a one-pot method with varying ratios of dopamine and BPA; D) XPS spectrum; E) TEM image, and F) related EDS spectrum of B-PDA nanoparticles.
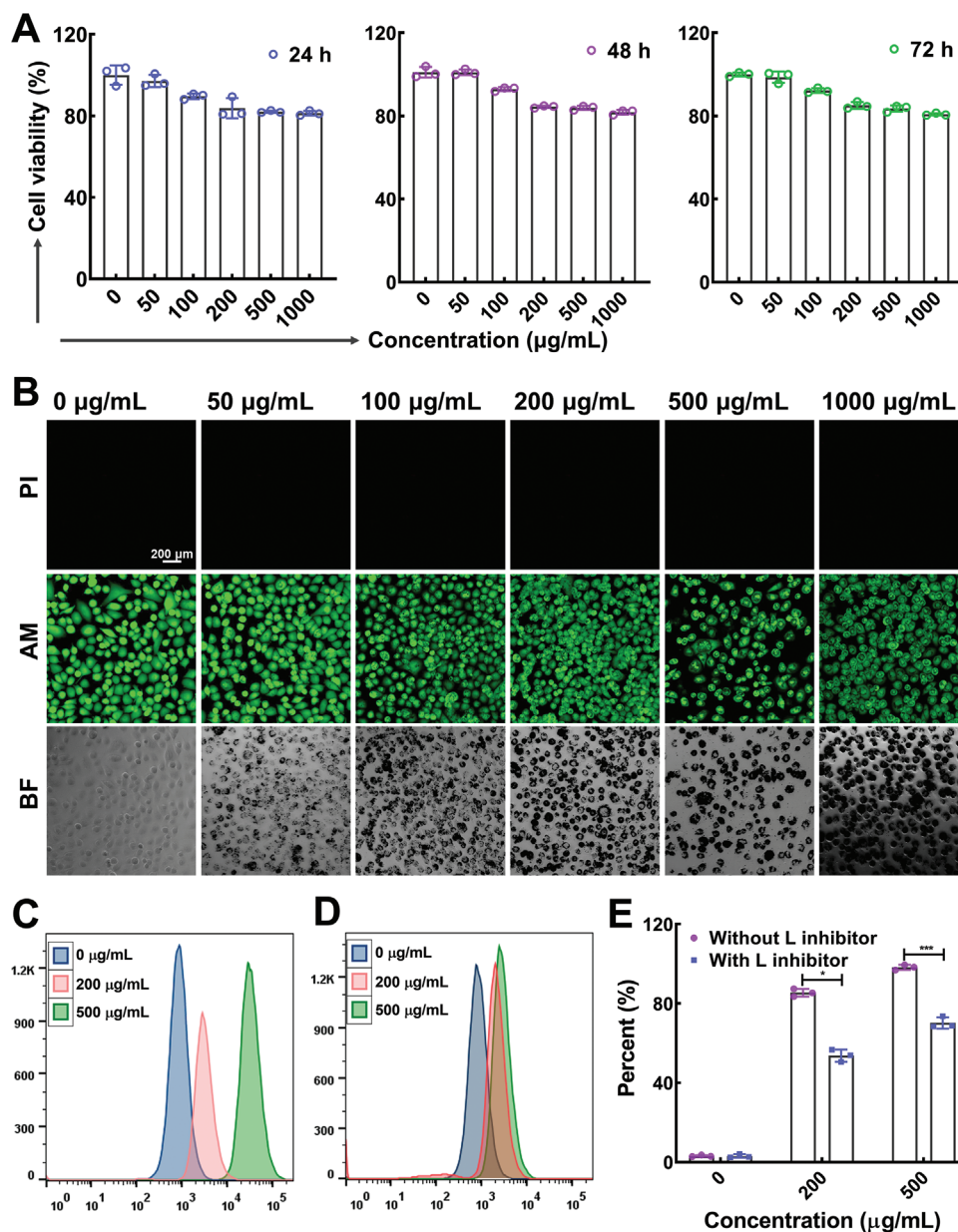
secondary structure, as shown in Figure S3A (Supporting Information), B-PDA showed a typcal FT-IR absorption bandwidth B-N stretching at 1388 cm$^{-1}$. Moreover, XPS was conducted to characterize the boron electronic states on B-PDA nanoparticles. The B 1 s spectrum of B-PDA was located at 192 eV (Figure 2D; Figure S3B, Supporting Information).

In the aqueous solution, B-PDA nanoparticles exhibited a narrow size distribution with an average hydrated particle size of 189 nm and a PDI of 0.040, as determined by DLS (Figure 2A), and the particle size in PBS and culture medium containing 10% FBS did not change distinctly (Figure S3C, Supporting Information). The surface charge density was determined by measuring the zeta potentials in H$_2$O, PBS and cell culture medium, and the results suggested that the zeta potentials were $-30 \pm 0.76$, $-21.89 \pm 0.74$, and $-19.91 \pm 0.55$ mV, respectively (Figure S3D, Supporting Information). Although B-PDA displayed a higher zeta potential when incubated with biological media, sufficient electrostatic repulsive force was provided to maintain the stability of a particle suspension.[27] As illustrated in Figure S3E (Supporting Information), no obvious change was observed during 24 h at 37 °C with various concentrations of B-PDA in the culture medium. SEM and TEM) images of the morphologies are shown in Figure 2B,E. B-PDA appeared as spherical particles ≈160 nm in diameter. Combining EDS and XPS (Figure 2D) results revealed the presence of boron. The EDS maps indicated that C, N, and B were colocalized with the nanoparticles (Figure 2F).

## 2.2. Cellular Uptake

A critically important index to evaluate the biocompatibility of biomaterials is cytotoxicity. Before cell uptake analysis, the U87 cell proliferation assay was conducted with a CCK8 kit, which showed no significant cytotoxicity between different concentration groups at 24, 48, and 72 h (**Figure 3**A). For the calcein-AM/PI assay, after treatment with various concentrations of B-PDA for 24 h, the cells were stained with calcein-AM and PI and imaged, and most samples emitted green fluorescence (Figure 3B). Similarly, consistent with the CCK8 assay results, the cells stained with calcein-AM and PI showed no toxicity. In addition, as shown in Figure 3B, as the concentration of B-PDA increased, more nanoparticles were taken up by U87 cells, which was observed in the bright field microscopy images. These results supported that the B-PDA nanoparticles were well tolerated and biologically compatible.

Additionally, efficient cell uptake is needed for BNCT-induced killing of cancer cells; thus, high and effective cellular uptake of B-PDA is a prerequisite for BNCT. Based on a previous report, LAT1 is regarded as a potential target protein for glioma therapy and is overexpressed in the blood-brain barrier.[21,28,29] We reasoned that the B-PDA nanoparticle phenylalanine residue from BPA might help to increase nanoparticle uptake in U87 cells by targeting LAT1. To validate this conjecture, we investigated the cellular uptake of

**ADVANCED
SCIENCE NEWS**

www.advancedsciencenews.com

**ADVANCED
FUNCTIONAL
MATERIALS**

www.afm-journal.de

**Figure 3.** Biosafety and cell uptake in vitro. A) In vitro cytotoxicity of B-PDA nanoparticles at various concentrations (1000, 500, 200, 100, 50, and 0 µg mL$^{-1}$, equivalent BPA 185, 93, 36.8, 18.5, 9.3, and 0 µg mL$^{-1}$ respectively) against U87 cells; B) calcein-AM/PI images of U87 cells incubated with different concentrations of B-PDA for 24 h; cellular uptake of Cy5@B-PDA evaluated by flow cytometric quantitative analysis in U87 cells when C) untreated with LAT1 inhibitor and D) pretreated with LAT1 inhibitor; E) statistical analysis of flow cytometric results. *P* values = *$P < 0.05$ and ***$P < 0.001$.

B-PDA nanoparticles when U87 cells were preincubated with or without the LAT1 inhibitor. As shown in Figure 3C,D, the cellular uptake of Cy5@B-PDA (Figure S4, Supporting Information) was significantly blocked by the LAT1 inhibitor. According to the flow cytometry analysis, which was performed to quantify the percentage of B-PDA uptake in U87 cells (Figure 3E), the cell uptake was reduced by half; this result was also demonstrated by fluorescence microscopy videos (Movies S1 and S2, Supporting Information). These results suggest that Cy5@B-PDA can efficiently enter cells by targeting LAT1.

## 2.3. The BNCT Efficacy Evaluation In Vitro

U87 cells were incubated with various concentrations of B-PDA for 24 h and washed three times with cell culture media, and then the boron contents of $1 \times 10^6$ cells were determined by ICP-MS. The intracellular boron concentrations reached $8.967 \pm 0.50$, $19.97 \pm 0.67$, and $32.64 \pm 0.40$ µg per $10^6$ cells when the B-PDA concentrations were 200, 500, and 1000 mg mL$^{-1}$, respectively (**Figure 4**A). This result indicated that the higher concentration of the nanoparticles resulted in a higher boron content of $1 \times 10^6$ U87 cells. When the B-PDA concentration
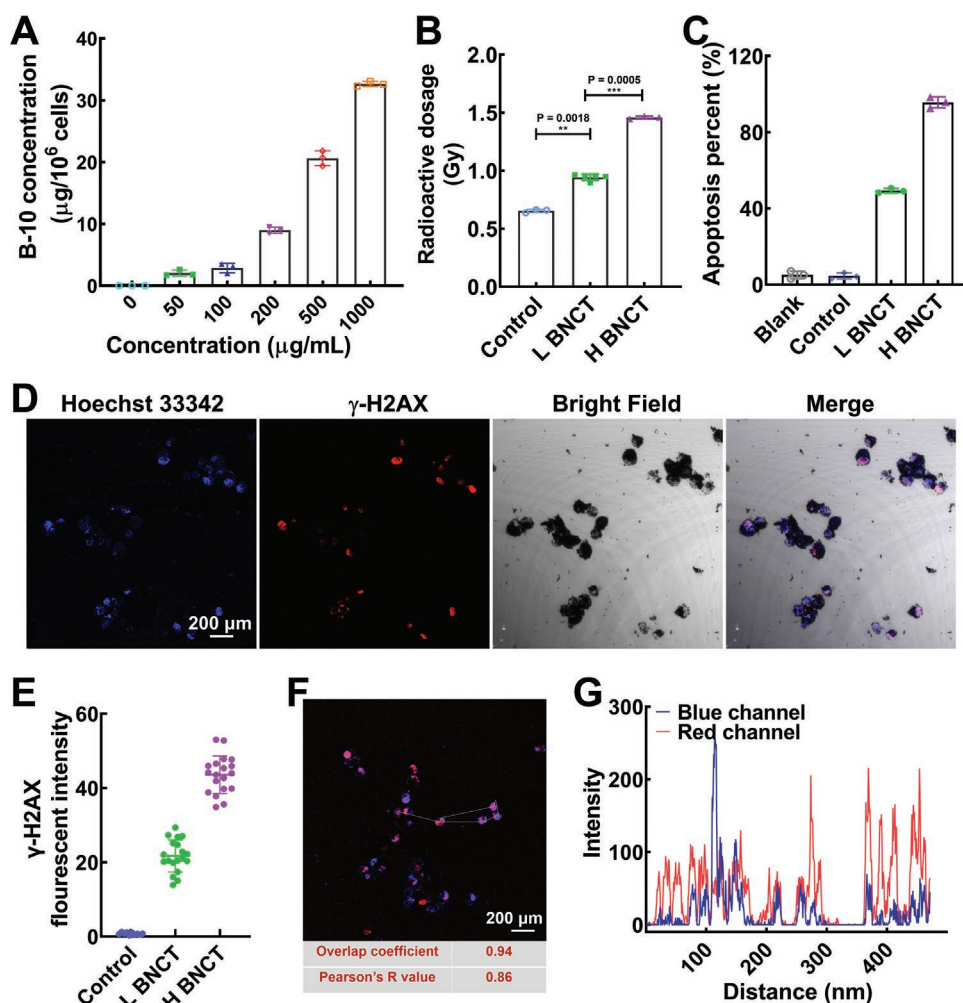
**Figure 4.** In vitro mechanistic studies of the B-PDA nanoparticles for BNCT in U87 cells. A) The boron concentrations of U87 cells incubated with B-PDA at different concentrations (1000, 500, 200, 100, 50, and 0 µg mL$^{-1}$, equivalent BPA 185, 93, 36.8, 18.5, 9.3, and 0 µg mL$^{-1}$ respectively); B) radiographic quantification post neutron irradiation; C) TUNEL staining was used to quantify apoptosis rates by flow cytometry analysis in vitro; D) representative immunofluorescence images of $\gamma$-H2AX in the H BNCT group; E) quantitative analysis of $\gamma$-H2AX immunofluorescence intensity in the experimental groups; F) colocalization analysis was performed using Zeiss Blue according to the wright line in the picture; G) red fluorescence channel of $\gamma$-H2AX colocalizing with the blue channel of cell nuclei.

was larger than 200 µg mL$^{-1}$, the intracellular boron content was sufficient to meet the BNCT requirements. These studies provide support for the feasibility of BNCT on cancer cells in vitro.

As described above, these results appeared to be sufficient to perform BNCT in vitro. To further demonstrate that B-PDA can realize robust efficacy against U87 cells as an excellent BNCT nanomedicine, U87 cells were preincubated with two concentrations (200 and 500 µg mL$^{-1}$) of B-PDA for 24 h. Then, the cells were harvested and collected in EP tubes, and finally exposed to neutron irradiation for 10 min. The cells untreated with B-PDA but irradiated with neutrons were set as the control group, and the normal cultured U87 cells were used as a blank control. The cells were placed on the apparatus when they received neutron irradiation, and the U87 cells within the dashed box were observed with the same dose neutron beam (Figure S5A, Supporting Information). Based on the previously mentioned boron content per 10$^6$ cells, the intracellular radioactivity dosage

was 1.41 ± 0.15, 0.95 ± 0.12, and 0.61 ± 0.17 Gy in the H BNCT (500 µg mL$^{-1}$ B-PDA), L BNCT (200 µg mL$^{-1}$ B-PDA) and control groups, respectively (Figure 4B). For the in vitro cell viability assay, the irradiated cells were seeded in 96-well plates at $1 \times 10^5$ cells per well and cultured for two days or seven days. The cell outlines were imaged by standard brightfield microscopy (Figure S5C, Supporting Information). The cells in the control group spread well and grew as clusters to form an adherent junction with the hub cells adjacent to them, which indicated that the cells remained in good physiological condition, while in the two additional BNCT groups, on the 2$^{nd}$ day, the cells mostly exhibited a round shape and were nonadherent; on the 7$^{th}$ day, the cell morphology of the L BNCT group gradually returned to normal, but this issue was not found in the H BNCT group. As illustrated in Figure S5B (Supporting Information), the CCK8 results showed that the proliferation of U87 cells in the H BNCT (500 µg mL$^{-1}$ B-PDA) and L BNCT (200 µg mL$^{-1}$ B-PDA) groups decreased to 21% and 52% on the 2$^{nd}$ day,

respectively, compared with that in the control group. On the 7th day, the cell proliferation in the LBNCT was higher than that on the 2nd day, there was no obvious significance in H BNCT. Additionally, the detection of apoptotic cells was performed using a TUNEL assay and flow cytometry. As shown in Figure 4C and Figure S5D (Supporting Information), a significant increase in apoptotic cells was discovered in both the H BNCT and L BNCT groups. The percentage of apoptotic U87 cells in the H BNCT and L BNCT groups was 94.86 ± 2.58% and 48.18 ± 3.08%, respectively, while no significant apoptosis induction was observed in the other two groups. Collectively, the results indicate that BNCT is a binary cancer therapy that requires a sufficient amount of boron within cells and that a low-energy neutron beam and B-PDA can be candidates for BPA delivery used in BNCT.[30]

The BNCT effect is usually attributed to double-strand DNA breaks inducing cell apoptosis. Hence, immunofluorescence staining of $\gamma$-H2AX was performed, counterstained with Hoechst 33342. The $\gamma$-H2AX fluorescence signal (red) indicated double-strand DNA damage (Figure S6, Supporting Information). The fluorescence quantitation analysis showed that the mean intensity was 38-fold higher in the H BNCT group and 25-fold higher in the L BNCT than in the control group (Figure 4E). Representative enlarged confocal microscopy showed nuclear blue staining and $\gamma$-H2AX red staining in H BNCT, and the cell nuclei showed chromatin condensation and nuclear fragmentation (Figure 4D). For colocalization analysis of $\gamma$-H2AX and the nucleus (Figure 4F), Pearson's coefficient was calculated using Zen Blue Software, which generated a coefficient of 0.94. Confocal analysis indicated that the $\gamma$-H2AX foci (red) and nucleus (blue) showed colocalization (Figure 4G). Therefore, these in vitro results all validated the efficacy of B-PDA for BNCT in U87 cells.

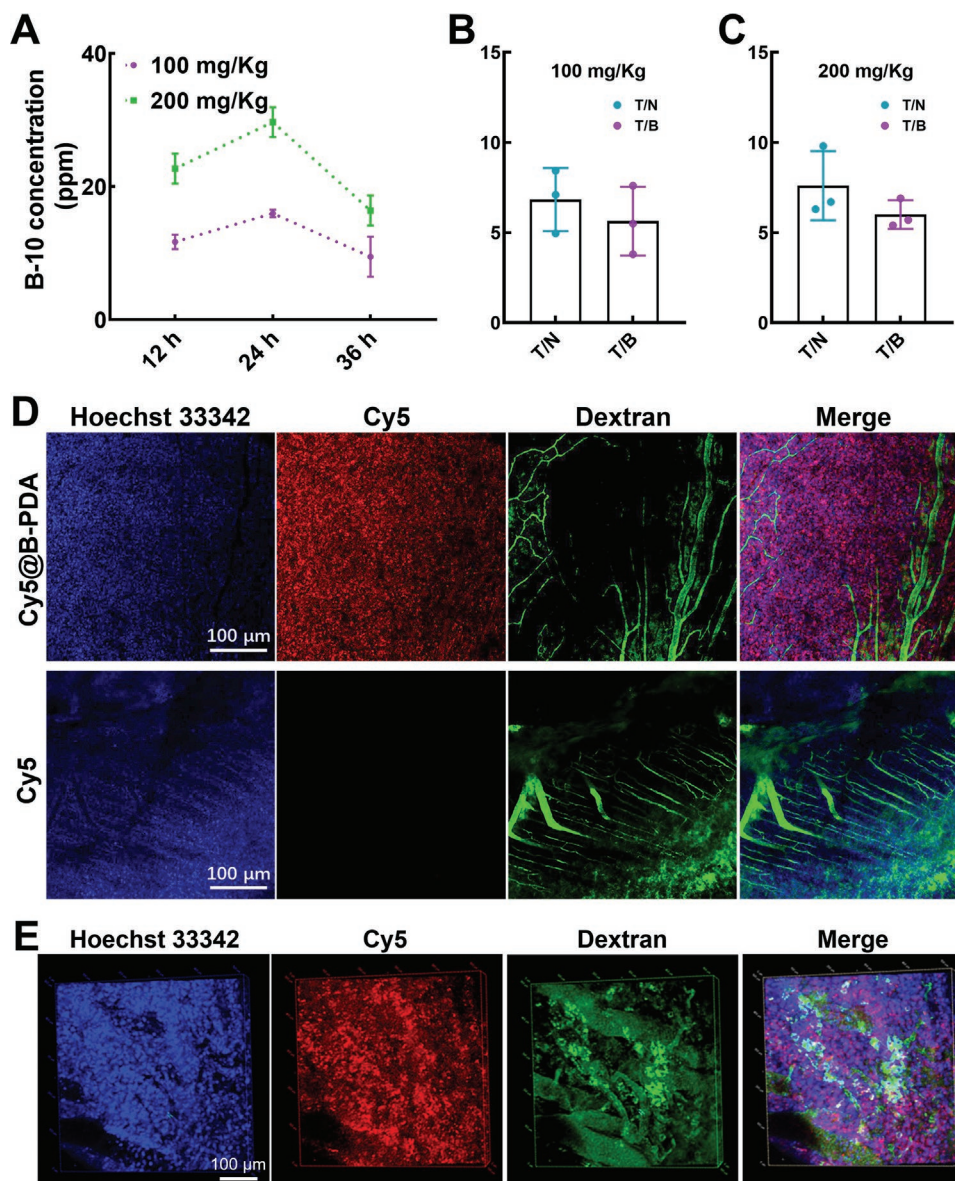### 2.4. B-PDA Distribution in Orthotopic Xenograft Glioma Mice

To further investigate the antitumor efficiency of B-PDA for BNCT in U87 glioma mice, we performed ICP-MS analysis to assess boron distribution in tissues in a mouse glioma model (Figure S7A–C, Supporting Information). According to the linear trend of boron concentration (**Figure** 5A), the boron content in tumor tissue reached a maximum of 15.95 ± 0.57 ppm and 29.68 ± 2.23 ppm at 24 h in the low-dose (100 mg kg$^{-1}$, $n$ = 3) and high-dose (200 mg kg$^{-1}$, $n$ = 3) groups, respectively. The boron concentrations in the high-dose groups were higher than those in the low-dose group at all indicated time points. In addition, it also suggested that B-PDA could realize efficient tumor accumulation and retention within tumor tissue. The tumor-to-blood (T/B) and tumor-to-normal tissue (T/N) ratios of the low dosage group were 5.63 ± 1.90 and 6.00 ± 0.79, respectively (Figure 5B); the corresponding values in the high dosage group were 6.83 ± 1.75 and 7.60 ± 1.91 (Figure 5C). Overall, the high-dose B-PDA nanoparticles satisfied the demands of the boron-containing drug for BNCT.

In addition, boron-based medicine must enter tumor cells as the "trigger" for BNCT to maximize antitumor efficiency in cancer treatment.[2] Herein, we used live fluorescence confocal imaging to investigate the relative distribution of Cy5@B-PDA in the tumor site at 24 h postinjection at a dosage of 200 mg kg$^{-1}$.

As shown in Figure 5D, although the tumor vessels were labelled with dextran-FITC and cell nuclei were tagged with Hoechst 33342 in the two groups, no red fluorescent signal was observed in the vicinity of Hoechst 33342-labelled cell nuclei; in contrast, in the Cy5@B-PDA group, the red fluorescent signal emitted by Cy5 was predominantly on the side of the cell nuclei marked by Hoechst 33342. This result also indicated that the nanoparticles could efficiently enter the cytoplasm. Moreover, the tumor site could be distinguished up to a depth of ≈200 µm (Figure 5E), which was possible because the B-PDA nanoparticles enabled effective accumulation in the tumor site and prolonged intracellular residence. In the tumor site, the vascular endothelium undergoes dysfunction and fenestration leading to the formation of leaky vessels, this phenomenon is the so-called enhanced permeation and retention (EPR) effect. Most nanoparticles can preferentially accumulate in tumor tissues via the EPR effect.[31] Moreover, cancer cells use different endocytosis mechanisms to internalize nanoparticles: phagocytosis; micropinocytosis and receptor-mediated endocytosis. The BPA residue of B-PDA also helps the nanoparticles entry into tumor cells. These properties result in the intra-tumoral trapping of the nanoparticles.

### 2.5. B-PDA for BNCT in Orthotopic Xenograft Glioma Mice

To further demonstrate the practicability of B-PDA nanoparticle-mediated BNCT regarding antitumor activity, we established an orthotopic xenograft model using Luc-U87 cells that could be visualized by luciferase bioluminescence. The animal experiments were conducted as illustrated in **Figure** 6A. The L BNCT and H BNCT groups were injected with B-PDA at doses of 100 and 200 mg kg$^{-1}$, respectively, while the control group was injected with saline. Twenty-four hours later, when the boron concentration reached the maximum (Figure 5A), the mice were fixed and received thermal neutron irradiation for 6 min. The fixation apparatus is shown in Figure 6B, and the neutron irradiation area is inside the white dashed circle. As shown in Figure 6D and Table S2 (Supporting Information), the mean radioactive dosage in the tumor site of H BNCT, L BNCT and control was 1.19, 0.88, and 0.32 Gy, respectively. In the H BNCT group, the radioactivity dose at tumor sites were 3.5 times greater than the dose for normal brain, while 2.6 times was observed in the L BNCT group and was not significantly different in the control group. Subsequently, all animals were imaged at 3, 5, and 10 days after neutron irradiation on an IVIS fluorescence imaging system. As demonstrated in Figure 6C, the fluorescence of tumor site intensity increased with time in the B-PDA, saline and control groups, suggesting that these groups showed no efficiency in tumor inhibition. Compared to L BNCT, H BNCT presented a superior anticancer effect, and there was only a weak signal observed on the 10th day in the H BNCT group. Magnetic resonance imaging (MRI) of the brain was performed on the 5th and 10th days, as illustrated in Figure 6E and Figure S8A (Supporting Information), and the results agreed with the live fluorescence imaging results. As determined with T1 and T2 images, regions of the tumor site showed no obvious signal enhancement in the H BNCT and were slightly larger in the L BNCT group but deteriorated with great dilation in the saline, B-PDA and control groups. Relative tumor volume

ADVANCED
SCIENCE NEWS
www.advancedsciencenews.com

ADVANCED
FUNCTIONAL
MATERIALS
www.afm-journal.de

**Figure 5.** Intratumor distribution of B-PDA nanoparticles. A) Boron concentrations of the tumor site after intravenous injection of B-PDA at different time points; the tumor-to-blood (T/B) ratios and tumor-to-normal tissue (T/N) ratios at 24 h at dosages of B) 100 mg kg$^{-1}$ (BPA dose: 18.5 mg kg$^{-1}$) and C) 200 mg kg$^{-1}$ (BPA dose: 37.0 mg kg$^{-1}$); D) live confocal microscope imaging of U87 glioma, red channel: Cy5@B-PDA, blue channel: cell nuclei, green channel: tumor vessel; E) 3D reconstructions of the live confocal fluorescent images.

over time in MRI was calculated as reported ($n$ = 3–6/group), and except for L BNCT and H BNCT, the tumor volumes in the groups increased ≈2.1 times. Compared with the three groups, the L BNCT group contained slower-growing tumors, but that of the H BNCT group did not show a significant increase (Figure 6F; Figure S8B,C, Supporting Information). These results urged us to examine whether B-PDA used in BNCT could prolong the survival of tumor-bearing mice. The statistical results were presented in Figure 6G. The B-PDA, saline and control groups' overall survival was less than 2 weeks, the median survival was 15 days in the L BNCT group, and the median survival was not reached in the H BNCT group. Collectively, H BNCT displayed the highest antitumor efficacy. Taken together, these results suggested that the B-PDA

nanoparticles were an efficient boron complex for BNCT in the U87 glioma tumor model.

This study also investigated the biological safety of B-PDA for BNCT in U87 tumor-bearing mice. Body weight was recorded during the experimental course (Figure 6H), and no significant change in mouse body weight was observed, which suggested that the treatments were well tolerated. Moreover, blood was collected from the orbital vein for CREA, ALB, AST, and ALT quantitative tests, and the renal and hepatic function indexes were within normal limits (Figure S9A,B, Supporting Information). The major organs (heart, liver, spleen, lung, kidney) were collected for haematoxylin and eosin (H&E) staining, and no obvious abnormalities were observed in the major organs (Figure S9C, Supporting Information).
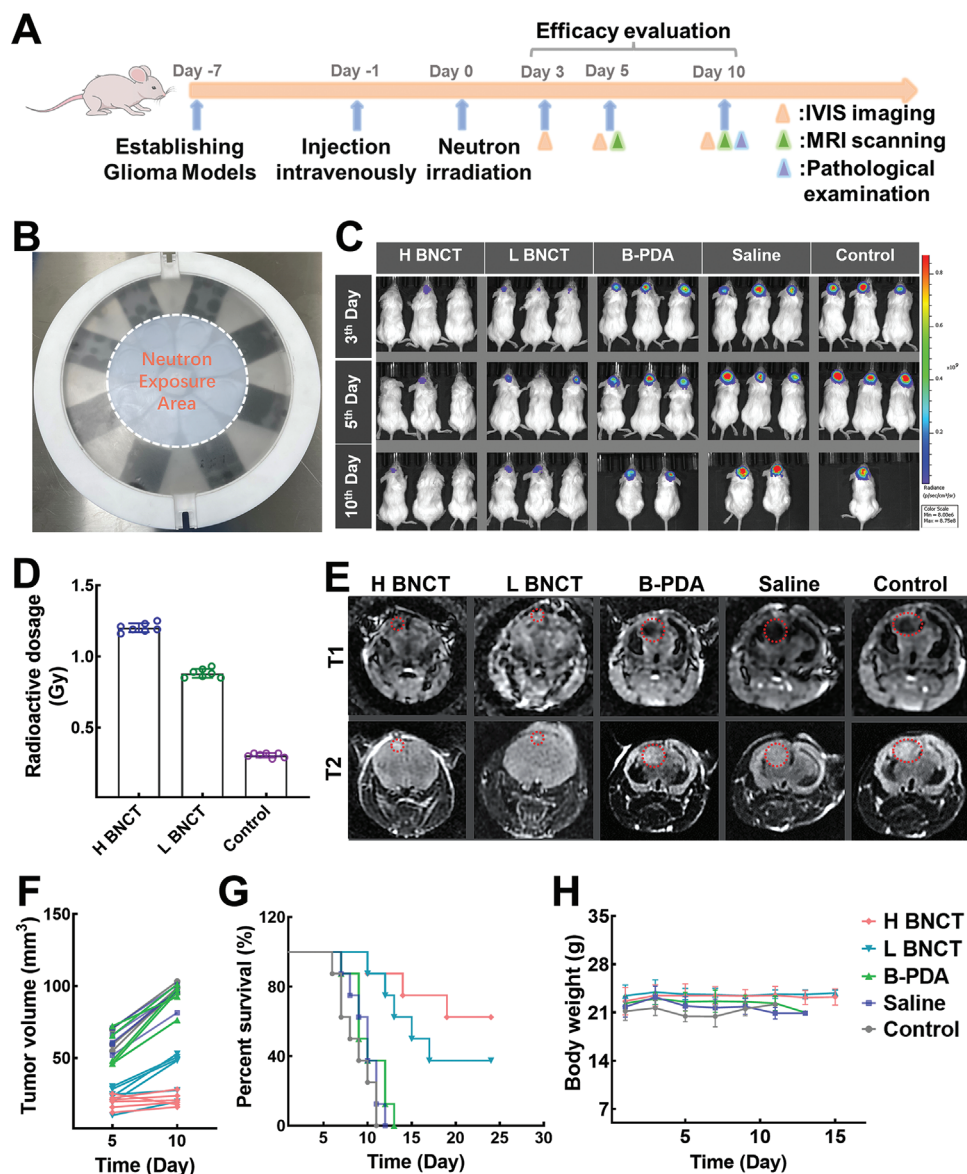
**Figure 6.** The antitumor efficacy of B-PDA for BNCT in orthotopic glioma. A) Flowchart of the overall experimental procedure for animals. B) Illustration of the mouse fixation apparatus. The mouse brain was fixed within the neutron exposure area when accepted with BNCT. C) Luciferase imaging was performed by an IVIS imaging system. D) Radioactive dose statistical analysis was performed using Monte Carlo. E) Representative MRI images on the 5th day after neutron irradiation. F) Changes in tumor volume was determined by MRI. G) The survival curve and H) body weight changes during the experimental period.

## 2.6. Pathological Examination

Considering the excellent initial results with the tumor inhibition effect, we further carried out a pathology analysis of brain tissues ex vivo. We evaluated the proliferation and apoptosis of tumor tissues via H&E staining, Ki67 staining, $\gamma$H2AX, and TUNEL staining. H&E staining showed a definitive demarcation of tumor tissue and normal brain tissue, and the tumor area in L BNCT and H BNCT was smaller than that of the three additional groups, but there was a metastatic lesion located in the third ventricle in the L BCNT group; in addition, the tumors expanded and eroded the sella and sphenoid sinus in the B-PDA, saline and control groups (**Figure** 7A).

Higher-magnification images of boxed areas showed that the cell nuclei displayed unsharp borders and fragmentation in the L BNCT and H BNCT groups. In contrast, intact cellular morphology and unbroken nuclei in the other three groups were observed, which was accompanied by a high percentage of Ki67-positive cells (Figure 7B). $\gamma$H2AX is regarded as a marker of DNA double-strand breaks induced by radiotherapy. To confirm the DNA double-strand breaks by BNCT, we also performed immunohistochemical analysis of $\gamma$H2AX, and the $\gamma$H2AX signal intensity in L BNCT and H BNCT was higher than that in the others (Figure 7C). In line with the results of $\gamma$H2AX staining, in situ TUNEL analysis showed increased apoptotic cells in the BNCT groups but no appreciable
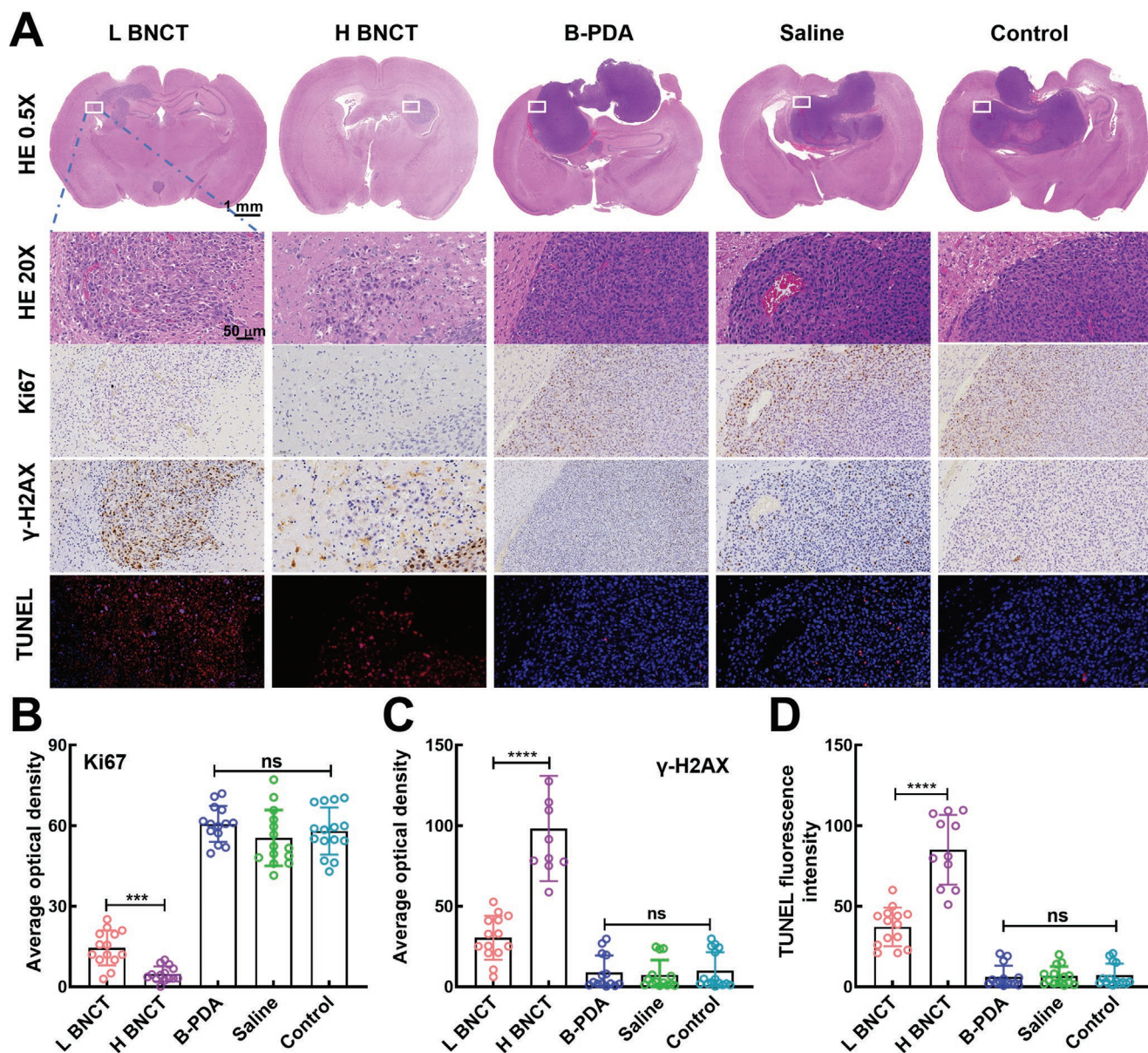
**Figure 7.** Results of pathological, immunohistochemical, and TUNEL staining examination. A) Representative pathological images of apoptosis and proliferation in tumor tissues in situ; statistical analysis of B) Ki67, C) $\gamma$-H2AX, and D) TUNEL staining. $P$ values = ****$p < 0.0001$; ***$p < 0.001$.

fluorescence in the other experimental groups (Figure 7D). Taken together, our study demonstrated that B-PDA nanoparticles can be used for BNCT and achieve an antitumor effect by breaking the DNA double-strands, inducing tumor cell apoptosis post neutron irradiation.

## 3. Discussion

Herein, our proof-of-concept experiments revealed that BPA-containing PDA nanoparticles could be fabricated via a one-pot method under alkaline conditions. Our design was based on the interactions between the boronic acid of BPA and the phenolic hydroxy group of dopamine. It was previously shown that

boronate esters were a versatile platform for drug delivery and nanomaterial preparation.[32,33] Additionally, the boronate ester could be formed under alkaline conditions (pH $\geq$ 7.5) and dissociated under acidic conditions (pH $\leq$ 5.5) or in the presence of $H_2O_2$, which mapped onto physiological pH conditions in vivo, allowing us to conclude that B-PDA nanoparticles could be enough stable during long circulation. Our experimental results demonstrated the formation of the boronate ester bond as shown in Figure S3A (Supporting Information) and the stability of B-PDA as shown in Figure S2E (Supporting Information).

In the clinic, a high boron concentration is crucial for BNCT application, and this requirement has limited the clinical utility of BNCT.[14] By changing the size, shape and material properties

**ADVANCED
SCIENCE NEWS**

www.advancedsciencenews.com

**ADVANCED
FUNCTIONAL
MATERIALS**

www.afm-journal.de

of the engineered nanoparticles, the degree of receptor cross-linking and subsequent cell responses can be precisely controlled, the abovementioned points would affect the accumulation at the tumor site.[34] As previously reported,[24,28] LAT1 is regarded as the active target of the blood-brain barrier and glioma cells. The B-PDA particles contained a phenylalanine residue, which would help the B-PDA nanoparticles cross the blood-brain barrier and recognize LAT1 for cell uptake and retention in cancer cells. To ascertain whether B-PDA enters U87 cells via LAT1-mediated transport, we further prepared Cy5@B-PDA, which was detected by flow cytometry. LAT1-dependent nanoparticle uptake was found, and the flow cytometry results showed high U87 cell uptake, which could be markedly reduced by preincubation with a LAT1 inhibitor (Figure 3C–E). Importantly, the biological safety of delivery platforms is necessary for BNCT. In addition, as one kind of artificially synthesized melanin, polydopamine presents high biosecurity, good biostability, and dispersibility.[35] We fabricated B-PDA nanoparticles using dopamine and BPA by a similar method, and the cell viability results from the pooled analysis revealed no obvious toxicity (Figure 3A,B), which suggested that the B-PDA nanoparticles could be a candidate for BNCT in glioma.

From previous reports, the fast metabolism and limited absorption of BPA in tumor sites resulted in a decrease in the magnitude of the BNCT effect.[1] In our studies, nanoparticles were introduced at a high dosage to meet the clinical demand of BNCT. Furthermore, previous studies have shown that nanomaterials can circulate for a long time to prolong retention in tumor sites. The boron accumulation at the tumor site was measured by ICP-MS and reached a maximum (29.68 ± 2.23 ppm) at 24 h postinjection (Figure 5A). At this moment, the concentration of boron in the tumor was 6.83-fold higher than that in blood and 7.60-fold higher than that in normal brain tissue (Figure 5B), which met the demands for BNCT. To study the intratumoral distribution of B-PDA in an orthotopic xenograft glioma model, we utilized live fluorescence imaging, and the results showed that B-PDA localized within tumor cells (Figure 5D,E). The satisfactory results might be attributed to two aspects. First, brain cells hardly divide at all; compared to normal brain cells, glioma cells show an uncontrolled increase in proliferation and metabolism, and therefore, they need a higher level of nutrients. During early tumor growth, one characteristic of U87 glioma is robust neovascularization to provide a supportive microenvironment for glioma cells.[36] Next, numerous studies indicate that various nanoparticles acting as drug carriers can preferentially accumulate in tumor tissues via the EPR effect to different extents. Additionally, LAT1 was reported to be overexpressed in U87 cells. The phenylalanine residue of B-PDA could recognize LAT1 to help nanoparticles enter cancer cells, which was demonstrated by our cell experiment result (Figure 3C–E). Collectively, the results indicated the potential of B-PDA use as a BNCT trigger for killing cancer cells.

Efficient enrichment in tumor cells does not represent an efficient antitumor effect. To this end, the antitumor efficacy of B-PDA for BNCT was assessed in vitro and in vivo. As mentioned in a previous study, BNCT induces DNA damage accompanied by $\gamma$H2AX foci.[37] In our studies, pathological examination indicated that BNCT largely induced DNA double-strand breaks to achieve excellent U87 cell killing and tumor ablation effects to prolong the survival of U87 tumor-bearing mice. Although our results, based on a limited record, suggest that this strategy has achieved the desired outcome, there are still some problems with B-PDA nanoparticles. Compared with the previous B-10 enriched nanoparticles,[38–44] our nanoparticles have a lower boron content, which led to more particles being injected to meet the demand of BNCT. Moreover, the metabolism, degradation and clearance performance of B-PDA nanoparticles were still determined, and the nanoparticle size was over 100 nm. Both scopes would induce particle enrichment in the spleen and be associated with potential systemic toxic side effects. These aspects need further investigation and improvement. Indeed, the mild effect of hyperthermia on enhancing tumor cell uptake can be attributed to the delivery of nanoparticles into the cytoplasm.[45] Polydopamine has an excellent photothermal conversion effect.[46] In future studies, we will further explore the photothermal conversion performance of B-PDA nanoparticles and investigate whether the hyperthermia effect will help B-PDA enter cells to reduce the dosage administered.

## 4. Conclusion

In this study, we successfully prepared BPA-doped B-PDA nanoparticles with good biocompatibility and stability by one-pot methods. These nanoparticles can cross the blood-brain barrier by targeting LAT1 to the site of the glioma tumor. The boron accumulation at the tumor site was measured by ICP-MS and reached a maximum (29.68 ± 2.23 ppm) 24 h postinjection. At this moment, the concentration of boron in the tumor was 6.8-fold higher than that in blood and 7.60-fold higher than that in normal brain tissue, which could meet the demands for BNCT. The antitumor efficacy of B-PDA for BNCT was assessed in vitro and in vivo. Based on the results above, it was clear that BNCT largely induced double-strand DNA breaks to achieve excellent U87 cell killing and tumor ablation effects. In summary, the B-PDA nanoparticles developed in this study showed great potential in the BNCT for U87-bearing tumor mice, and their ability to become promising agents for clinical BNCT can be tested in further experiments. We also hope that this work will encourage and convince more scientists to devote new creative efforts to pharmaceutical agents for BNCT.

## 5. Experimental Section

*Reagents and Apparatus*: All reagents and chemicals were purchased from Sigma-Aldrich, J&K Scientific, TCI, Energy Chemical, and Bide Pharm. The other cell culture reagents were purchased from Gibco and HyClone. Cell fluorescence imaging was recorded by a single-confocal laser imaging system (Zeiss LSM880, Germany), and animal fluorescence imaging was performed by Nikon (A1R+MP, Japan). Scanning electron microscopy (SEM, Thermo Scientific, Apreo 2C), transmission electron microscopy (TEM, Thermo Scientific, Talos F200S), and other characterization analyses of the material samples were conducted at the Analysis and Testing Center, Sichuan University. Particle size, polydispersity (PDI), and the surface zeta potential were characterized by dynamic light scattering (DLS, Malvern 2000). The neutron irradiation experiments were supported by Neuboron Medtech. Ltd. (Nanjing, China).

*Preparation of B-PDA Nanoparticles*: Dopamine and BPA were susceptible to self-polymerization, which produced a series of BPA-containing PDA (BPA-PDA) nanoparticles at different mass ratios (dopamine: BPA = 1:1, 2:1, 3:1, 4:1, 5:1). The mixture was stirred at a mass concentration of 2 mg mL$^{-1}$ in aqueous solution (pH = 10.0) for 12 h to prepare the nanoparticles. The nanoparticles were isolated via centrifugation at 10 000 rpm for 10 min and washed with deionized water three times. Finally, the product was redispersed in water and placed at room temperature for the following experiments.

*Characterization of B-PDA Nanoparticles*: BPA-PDA with different raw material ratios was fabricated according to the methods above. All the products, differing in the ratio of BPA, were investigated in this study by inductively coupled plasma-mass spectrometry (ICP-MS, Thermo Scientific, ICAP RQ) to analyze the percent of BPA. The particle size, zeta potential and PDI in the hydrated condition, samples were subjected to DLS analysis. The particle size and morphology were recorded by SEM and TEM. X-ray photoelectron spectroscopy (XPS, Thermo Fischer, ESCALAB 250Xi) was used to characterize the surface chemistry of B-PDA. Energy dispersive spectroscopy (EDS, Thermo Fischer, FEI Talos F200S, Super-X) spectra were obtained to confirm the chemical element composition. Two days prior to the in vitro and in vivo experiments, the B-PDA nanoparticles were prepared and then resuspended in PBS.

*Preparation of Cy5@B-PDA*: To graft Cy5, B-PDA nanoparticles were suspended in water at a concentration of 1 mg mL$^{-1}$, and Cy5 was added to the reaction solution at a mass ratio of 1:1. The solution was then stirred for 12 h. The products were isolated and purified via centrifugation at 10 000 rpm for 10 min and washed with deionized water three times. To ensure the grafting of Cy5 onto the surface of the B-PDA nanoparticles, the fluorescence emission spectra of the Cy5 labelled B-PDA particles were verified with a spectrophotometer.

*Cell Culture and Animals*: U87 cells were maintained in Dulbecco's modified Eagle's medium (DMEM) containing 10% bovine calf serum (HyClone, Logan, UT) and cultured at 37 °C in a 5% CO$_2$ incubator. NCG mice (5 weeks old, 20 g in weight) were purchased from Gempharmatech Co., Ltd. and housed in sterile barrier conditions in 12 h light/12 h dark cycles according to the animal care facility at Sichuan University. All animals were maintained for at least one week to acclimatize to the environment and reduce stress before all animal experiments. For the orthotopic xenograft glioma model, orthotopic glioma tumors were established by intracranial injection of $1 \times 10^5$ Luc-U87 cells (luciferase-positive) in a total volume of 5 μL into the brains of NCG mice. The IVIS live imaging system was used to ensure tumor engraftment and monitor tumors on the 5$^{th}$ day post-injection. When the glioma model in situ was successfully established, the mice were randomly grouped according to the experimental design. Tumor growth was recorded by magnetic resonance imaging (MRI) every five days during the efficiency evaluation. All in vivo experiments were approved by the Animal Care and Use Committee and Ethics Committee of West China Hospital, Sichuan University (20220223053).

*Cellular Uptake*: For CCK8 cytotoxicity analysis, U87 cells were plated in 96-well plates and cultured for 24 h. Then, culture medium was removed, and DMEM containing different concentrations (1000, 500, 200, 100, 50, and 0 μg mL$^{-1}$) of B-PDA nanoparticles was added, and the cells were processed according to the CCK8 manufacturer's instructions (Dojindo, Japan) before being quantified on a microplate reader (TECAN SPARK, USA). Furthermore, the cytotoxicity of B-PDA was evaluated using calcein-AM/PI.

In addition, for boron concentration assays, U87 cells were cultured in 10-cm dishes and allowed to reach a density of 70%–80% on the subsequent day. Then, the culture medium containing different B-PDA concentrations (1000, 500, 200, 100, 50, and 0 μg mL$^{-1}$, equivalent BPA 185, 93, 36.8, 18.5, 9.3, and 0 μg mL$^{-1}$ respectively) was added, and the cells were incubated for another 24 h. The cells were washed with PBS three times, harvested by trypsinization, washed with fresh culture medium and counted, and $1 \times 10^6$ cells were finally resuspended in 500 μL nitric acid for digestion. Boron contents in $1 \times 10^6$ cells treated with different concentrations were measured by ICP-MS in triplicate.

*Examination of LAT1 Targeting*: U87 cells were seeded in 6-cm dishes for 24 h at a density of ≈70–80%. Cy5@B-PDA (200 or 500 μg mL$^{-1}$, equivalent BPA 93 or 36.8 μg mL$^{-1}$ respectively) was added to the cells and incubated for 4 h. In parallel, the U87 cells were pretreated with the LAT1 inhibitor (2-aminocyclclo-(2,2,1)-heptane-2-carboxylic acid, 10 mM) 2 h before the addition of B-PDA nanoparticles. After briefly being washed with cold PBS three times, the cells were collected and analyzed by flow cytometry. In addition, the cellular uptake of Cy5@B-PDA nanoparticles (500 μg mL$^{-1}$) was recorded by confocal imaging microscopy.

*B-PDA Distribution In Vivo*: For the pharmacokinetic study, one group was injected with B-PDA nanoparticles (100 mg kg$^{-1}$, equivalent BPA 18.5 mg kg$^{-1}$) via the tail vein (n = 3/group), and the other group was also injected with nanoparticles (200 mg kg$^{-1}$, equivalent BPA 37.0 mg kg$^{-1}$) via the tail vein. After long cycle times, the mice were sacrificed, and major organs (heart, liver, spleen, lung, kidneys, brain), blood and tumors were retrieved and measured for wet weights immediately. Then, quantitative analysis of boron content in these organs and tissues was monitored by ICP-MS. For ICP-MS, organs were digested with 5 mL 60% nitric acid at 90 °C for 12 h, diluted to 30 mL with deionized water and processed.

Based on the B-PDA distribution in vivo, the intratumoral distribution of B-PDA nanoparticles was further monitored by live fluorescence confocal imaging. The peak boron concentration in the tumor site, which was determined by ICP-MS, was identified as the time point for imaging. To this end, the mice were injected with Hoechst 33342 (5 mg kg$^{-1}$) and dextran-FITC (Mw: 170 kDa, 5 mg kg$^{-1}$) via the tail vein 30 min before imaging. For live-imaging experiments, the mice were euthanized, the hairs were shaved, and the skull was resected to expose the tumor site. The pictures were recorded by upright single-photon confocal microscopy (Nikon A1R+MP, Japan).

*Efficacy Assessments of BNCT on U87 Cells*: All cell or animal irradiation experiments were completed at Xiamen Humanity Hospital-Neuboron BNCT Center based on the NeuPex$^{TM}$ Block-I AB-BNCT system. A total of $5 \times 10^6$ U87 cells were seeded in 10-cm dishes, allowed to adhere and grow for another 24 h, and then incubated with different concentrations (0, 200, and 500 μg mL$^{-1}$) of B-PDA for 24 h in a 37 °C incubator. The cells were then washed with PBS, collected by trypsin digestion and washed three times with DMEM containing 10% FBS. Before neutron irradiation, all cells treated with different doses of B-PDA were suspended in 200 μL culture medium and transferred to an Eppendorf tube with a volume of 0.6 mL, and finally subjected to neutron irradiation for 10 min (Epithermal Neutron Flux: $8.015 \times 10^8$ n cm$^{-2}$ s$^{-1}$). Subsequently, the cells were secondarily cultured for two days or seven days and used for efficacy evaluation in vitro. To gauge cell apoptosis on the 2$^{nd}$ day, the apoptotic cells were detected by a TUNEL assay according to the manufacturer's instructions and finally quantitated by flow cytometry.

For $\gamma$-H2AX staining, the cells were washed with PBS three times and fixed with 4% PFA for 10 min at room temperature. Then, the cells were washed with PBS, treated with 5% FBS for 30 min and subjected to 0.3% Triton X-100 in PBS for 10 min at room temperature. The supernatant was aspirated, and rabbit anti-rat $\gamma$-H2AX primary antibody (CST, 50 mL, 1:200) was added and incubated for another 2 h at 37 °C. The cells were washed with PBS and incubated with goat anti-rabbit Alexa Fluor 647 secondary antibody (CST, 50 mL, 1:1000) for 1 h at 37 °C, and then the nucleus was stained with Hoechst 33342. After a brief washing with PBS, images were recorded by a Zeiss 880 laser scanning microscope.

*BNCT in Orthotopic Xenograft Glioma Mice In Vivo*: On day 7 after the U87 cells were injected, the animals were pooled and randomly divided into five groups (n = 8/group) with comparable average tumor size, and the tumor volume was determined by multiplying the average intensity of fluorescence using the 2D image area. The low-dose (100 mg kg$^{-1}$, equivalent BPA 18.5 mg kg$^{-1}$) and high-dose groups (200 mg kg$^{-1}$, equivalent BPA 37.0 mg kg$^{-1}$) were administered to the mice through tail vein injection 24 h before neutron irradiation. The other three experimental groups were subjected to the following procedures: the B-PDA group (200 mg kg$^{-1}$) was injected with B-PDA via tail vein injection without neutron irradiation, the control group was intravenously administered 200 μL saline and irradiated with neutron beams, and the

saline group animals were intravenously administered 200 μL saline. The mice were anaesthetized by intraperitoneal injection of a mixture of 100 mg kg$^{-1}$ ketamine and 10 mg kg$^{-1}$ xylazine under aseptic conditions. After 3–5 min, the animals were deeply anaesthetized and immobilized on the specific body fixation apparatus and then irradiated for ≈6 min on the NeuPex$^{TM}$ Block-I AB-BNCT system (Epithermal Neutron Flux: $8.015 \times 10^8$ n cm$^{-2}$ s$^{-1}$). The mice were returned to the conditioning boxes for the following experiments.

*Evaluation of Antitumor Efficiency*: To monitor tumor growth in vivo, the head of individual mice was detected by 3.0T MRI (GE SIGNA 3.0T, Germany) via T1-weight imaging (T1WI) (TR: 12.2 ms, TE: 4.0 ms, thickness: 0.2 mm, scan time: 6 min 13 s) and T2-weight imaging (T2WI) sequences (TR: 10 000 ms, TE: 140 ms, thickness: 0.9 mm, scan time: 6 min 50 s) every 5 days, and at the same time, bioluminescence imaging was performed using an IVIS imaging system on days 3, 5, and 10. During the experiment, natural survival was recorded, and blood was collected from the orbital sinus of mice for biochemical assays.

One mouse from each group was sacrificed on the 10$^{th}$ day postirradiation, and the other major organs (heart, liver, spleen, lung, kidney) were harvested and embedded in paraffin, serially sectioned into ≈5 μm slices and stained with haematoxylin and eosin (H&E) according to the standard procedures for the detection of histological lesions by light microscopy. The tumor tissues were isolated and fixed for H&E, TUNEL and Ki67 staining for pathological analysis, and a total of 6–8 randomly selected sections per animal were quantified.

*Radiation Dose Calculation for the In Vitro and In Vivo Experiments*: Cells and mice were irradiated by using the accelerator-based BNCT system NeuPex (https://en.neuboron.com/products) developed by Neuboron Therapy System Ltd., in Xiamen, China. The neutron accelerator voltage is 2.3 MeV, and the current is 7 mA. The cells or mice were fixed in the corresponding holder while the holder was mounted into the irradiation port for irradiation. The cell holder as well as the mouse holding device were carefully designed to provide a uniform, low-contamination, high-intensity thermal neutron field to the targets.

To estimate the received dose accurately, the mouse and cell experiments were carefully modelled and calculated by using the Monte Carlo method. Radiation doses were calculated using the Monte Carlo toolkit PHITS (ver. 3.16) combined with the ENDF/B-VIII.0 cross section library.[47,48] The calculation model included the neutron source, beam shaping assembly, irradiation port, and irradiated device, including cells/mice in the model. The neutron beam model was created according to a detailed geometric description of the NeuPex AB-BNCT system. A uniform layer 10 μm thick was constructed as a cell model. The mouse model was constructed by using a voxel model and the lattice tally method,[49] in which the corresponding organ at risk information was retrieved from real CT images (Figure S1, Supporting Information). Elemental composition and density data from ICRU 46 were used.[50] The treatment planning system NeuMANTA (Neuboron Multifunctional Arithmetic for Neutron Transportation Analysis, NeuMANTA) was applied for region of interest contouring purposes (Figure S1, Supporting Information).[51] The boron dose was calculated using the boron concentration information measured from biosamples, as explained in other sections. On this basis, the physical dose components of the cells or mice were calculated.

*Statistical Analysis*: All slices were analyzed by ImageJ, and all data are expressed as the mean ± standard deviation. For two groups, Student's $t$ was performed, and analysis of variance (ANOVA) was performed for multiple groups. Differences with a $p < 0.05$ were considered significant. The statistical analysis was performed using GraphPad Prism 7.0.Acknowledgments

## Supporting Information

Supporting Information is available from the Wiley Online Library or from the author.

## Conflict of Interest

The authors declare no conflict of interest.

## Data Availability Statement

The data that support the findings of this study are available from the corresponding author upon reasonable request.

## Keywords

[1] R. F. Barth, J. A. Coderre, M. G. H. Vicente, T. E. Blue, *Clin. Cancer Res.* **2005**, *11*, 3987.

[2] M. A. Dymova, S. Y. Taskaev, V. A. Richter, E. V. Kuligina, *Cancer Commun.* **2020**, *40*, 406.

[3] R. F. Barth, Z. Zhang, T. Liu, *Cancer Commun.* **2018**, *38*, 36.

[4] A. H. Soloway, W. Tjarks, B. A. Barnum, F. G. Rong, J. G. Wilson, *Chem. Rev.* **1998**, *98*, 1515.

[5] K. Kawai, K. Nishimura, S. Okada, S. Sato, M. Suzuki, T. Takata, H. Nakamura, *Mol. Pharmaceutics* **2020**, *17*, 3740.

[6] Y. Hashimoto, F. Hiraga, Y. Kiyanagi, *Appl. Radiat. Isot.* **2015**, *106*, 88.

[7] L. Porra, L. Wendland, T. Seppälä, H. Koivunoro, H. Revitzer, J. Tervonen, L. Kankaanranta, A. Anttonen, M. Tenhunen, H. Joensuu, *Cancer Biother.Radiopharm.* **2022**, https://doi.org/10.1089/cbr.2022.0059.

[8] K. Ono, S. Ueda, Y. Oda, Y. Nakagawa, S. Miyatake, M. Osawa, T. Kobayashi, in *Boron Neutron Capture Therapy for Malignant Glioma at Kyoto University Reactor*, (Eds: B. Larsson, J. Crawford, J. Weinreich) Elsevier Science, Amsterdam **1997**, *1*, 39.

[9] H. Joensuu, L. Kankaanranta, T. Seppälä, I. Auterinen, M. Kallio, M. Kulvik, J. Laakso, J. Vähätalo, M. Kortesniemi, P. Kotiluoto, T. Serén, J. Karila, A. Brander, E. Järviluoma, P. Ryynänen, A. Paetau, I. Ruokonen, H. Minn, M. Tenhunen, J. Jääskeläinen, M. Färkkilä, S. Savolainen, *J. Neuro-Oncol.* **2003**, *62*, 123.

[10] A. D. Chanana, J. Capala, M. Chadha, J. A. Coderre, A. Z. Diaz, E. H. Elowitz, J. Iwai, D. D. Joel, H. B. Liu, R. Ma, N. Pendzick, N. S. Peress, M. S. Shady, D. N. Slatkin, G. W. Tyson, L. Wielopolski, *Neurosurgery* **1999**, *44*, 1182.

[11] Y.-W. H. Liu, T. T. Huang, S. H. Jiang, H. M. Liu, *Appl. Radiat. Isot.* **2004**, *61*, 1039.

[12] L.-W. Wang, Y.-W. H. Liu, F.-I. Chou, S.-H. Jiang, *Cancer Commun.* **2018**, *38*, 37.

[13] K. Hu, Z. Yang, L. Zhang, L. Xie, L. Wang, H. Xu, L. Josephson, S. H. Liang, M. R. Zhang, *Coord. Chem. Rev.* **2020**, *405*, 213139.

[14] M. Lamba, A. Goswami, A. Bandyopadhyay, *Chem. Commun.* **2021**, *57*, 827.

[15] R. F. Barth, W. Yang, G. Wu, M. Swindall, Y. Byun, S. Narayanasamy, W. Tjarks, K. Tordoff, M. L. Moeschberger, S. Eriksson, P. J. Binns, K. J. Riley, *Proc. Natl. Acad. Sci. USA* **2008**, *105*, 17493.

[16] W. Chen, S. C. Mehta, D. R. Lu, *Adv. Drug Delivery Rev.* **1997**, *26*, 231.

[17] G. Choi, I.-R. Jeon, H. Piao, J.-H. Choy, *Adv. Funct. Mater.* **2018**, *28*, 1704470.

[18] A. Kim, M. Suzuki, Y. Matsumoto, N. Fukumitsu, Y. Nagasaki, *Biomaterials* **2021**, *268*, 120551.

[19] W. Islam, Y. Matsumoto, J. Fang, A. Harada, T. Niidome, K. Ono, H. Tsutsuki, T. Sawa, T. Imamura, K. Sakurai, N. Fukumitsu, H. Yamamoto, H. Maeda, *Biomaterials* **2021**, *269*, 120631.

[20] J. Li, J. Kong, S. Ma, J. Li, M. Mao, K. Chen, Z. Chen, J. Zhang, Y. Chang, H. Yuan, T. Liu, Z. Zhang, G. Xing, *Adv. Funct. Mater.* **2021**, *31*, 2100969.

[21] A. Detta, G. S. Cruickshank, *Cancer Res.* **2009**, *69*, 2126.

[22] P. C. Huszthy, I. Daphu, S. P. Niclou, D. Stieber, J. M. Nigro, P. Ø. Sakariassen, H. Miletic, F. Thorsen, R. Bjerkvig, *Neuro-Oncology* **2012**, *14*, 979.

[23] K. Lenting, R. Verhaak, M. T. Laan, P. Wesseling, W. Leenders, *Acta Neuropathol.* **2017**, *133*, 263.

[24] M. B. Nodwell, Y. Hua, M. Čolović, Z. Yuan, H. Merkens, R. E. Martin, F. Bénard, P. Schaffer, R. Britton, *J. Am. Chem. Soc.* **2017**, *139*, 3595.

[25] A. Stubelius, S. Lee, A. Almutairi, *Acc. Chem. Res.* **2019**, *52*, 3108.

[26] H. Ueda, M. Suzuki, R. Kuroda, T. Tanaka, S. Aoki, *J. Med. Chem.* **2021**, *64*, 8523.

[27] G. M. Arepally, R. Qi, J. Hollingsworth, S. Suvarna, *Blood* **2006**, *108*, 96.

[28] K. Morrison, *Neuro-Oncology* **2022**, *24*, iv5.

[29] M.-F. Paugam, L. S. Valencia, B. Boggess, B. D. Smith, *J. Am. Chem. Soc.* **1994**, *116*, 11203.

[30] S.-I. Miyatake, S. Kawabata, H. Goto, Y. Narita, M. Suzuki, K. Hirose, Y. Takai, K. Ono, T. Ohnishi, H. Tanaka, T. Kato, *J. Clin. Oncol.* **2020**, *38*, 2536.

[31] Z. Zhao, A. Ukidve, J. Kim, S. Mitragotri, *Cell* **2020**, *181*, 151.

[32] S. Lv, Y. Wu, K. Cai, H. He, Y. Li, M. Lan, X. Chen, J. Cheng, L. Yin, *J. Am. Chem. Soc.* **2018**, *140*, 1235.

[33] C. Liu, T. Wan, H. Wang, S. Zhang, Y. Ping, Y. Cheng, *Sci. Adv.* **2019**, *5*, eaaw8922.

[34] E. Blanco, H. Shen, M. Ferrari, *Nat. Biotechnol.* **2015**, *33*, 941.

[35] W. Cao, X. Zhou, N. C. McCallum, Z. Hu, Q. Zhe Ni, U. Kapoor, C. M. Heil, K. S. Cay, T. Zand, A. J. Mantanona, A. Jayaraman, A. Dhinojwala, D. D. Deheyn, M. D. Shawkey, M. D. Burkart, J. D. Rinehart, N. C. Gianneschi, *J. Am. Chem. Soc.* **2021**, *143*, 2622.

[36] C. A. Madigan, C. J. Cambier, K. M. Kelly-Scumpia, P. O. Scumpia, T.-Y. Cheng, J. Zailaa, B. R. Bloom, D. B. Moody, S. T. Smale, A. Sagasti, R. L. Modlin, L. Ramakrishnan, *Cell* **2017**, *170*, 973.

[37] J. Li, Q. Sun, C. Lu, H. Xiao, Z. Guo, D. Duan, Z. Zhang, T. Liu, Z. Liu, *Nat. Commun.* **2022**, *13*, 2143.

[38] N. Kuthala, R. Vankayala, Y.-N. Li, C.-S. Chiang, K. C. Hwang, *Adv. Mater.* **2017**, *29*, 1700850.

[39] Y. Wang, G. Reina, H. G. Kang, X. Chen, Y. Zou, Y. Ishikawa, M. Suzuki, N. Komatsu, *Small* **2022**, *18*, 2204044.

[40] M. W. Mortensen, O. Björkdahl, P. G. Sørensen, T. Hansen, M. R. Jensen, H. J. G. Gundersen, T. Bjørnholm, *Bioconjugate Chem.* **2006**, *17*, 284.

[41] L. Li, J. Li, Y. Shi, P. Du, Z. Zhang, T. Liu, R. Zhang, Z. Liu, *ACS Nano* **2019**, *13*, 3843.

[42] D. Kozień, B. Szermer-Olearnik, A. Rapak, A. Szczygieł, N. Anger-Góra, J. Boratyński, E. Pajtasz-Piasecka, M. M. Bućko, Z. Pędzich, *Materials* **2021**, *14*, 3010.

[43] W. M. Silva, H. Ribeiro, J. J. Taha-Tijerina, *Nanomaterials* **2021**, *11*, 2907.

[44] A. Zaboronok, P. Khaptakhanova, S. Uspenskii, R. Bekarevich, L. Mechetina, O. Volkova, B. J. Mathis, V. Kanygin, E. Ishikawa, A. Kasatova, D. Kasatov, I. Shchudlo, T. Sycheva, S. Taskaev, A. Matsumura, *Pharmaceutics* **2022**, *14*, 761.

[45] J. Wu, G. R. Williams, S. Niu, F. Gao, R. Tang, L.-M. Zhu, *Adv. Sci.* **2019**, *6*, 1802001.

[46] Y. Zou, X. Chen, P. Yang, G. Liang, Y. Yang, Z. Gu, Y. Li, *Sci. Adv.* **2020**, *6*, eabb4696.

[47] K. Niita, T. Sato, H. Iwase, H. Nose, H. Nakashima, L. Sihver, *Radiat. Meas.* **2006**, *41*, 1080.

[48] D. A. Brown, M. B. Chadwick, R. Capote, A. C. Kahler, A. Trkov, M. W. Herman, A. A. Sonzogni, Y. Danon, A. D. Carlson, M. Dunn, D. L. Smith, G. M. Hale, G. Arbanas, R. Arcilla, C. R. Bates, B. Beck, B. Becker, F. Brown, R. J. Casperson, J. Conlin, D. E. Cullen, M.-A. Descalle, R. Firestone, T. Gaines, K. H. Guber, A. I. Hawari, J. Holmes, T. D. Johnson, T. Kawano, B. C. Kiedrowski, et al., *Nucl. Data Sheets* **2018**, *148*, 1.

[49] Y.-H. Liu, P.-Y. Lee, Y.-C. Lin, F.-I. Chou, W.-L. Chen, Y.-S. Huang, S.-H. Jiang, *Appl. Radiat. Isot.* **2014**, *88*, 125.

[50] J. A. Scott, *J. Nucl. Med.* **1993**, *34*, 171.

[51] J. Chen, Y.-C. Teng, W.-B. Zhong, H.-B. Yang, Q. Hong, Y.-H. Liu, *J. Phys.: Conf. Ser.* **2022**, *2313*, 012012.